Operating Grid-Forming Control on Automotive Reversible Battery Charger

Yorgo Laba, Antoine Bruyere, Frederic Colas, Xavier Guillaud, Bénédicte Silvestre

Operating Grid-Forming Control on Automotive Reversible Battery Charger

Yorgo Laba[1,3] yorgo.laba@centralelille.fr
Antoine Bruyère[1,3] antoine.bruyere@centralelille.fr
Frédéric Colas[1,2] frederic.colas@ensam.eu
Xavier Guillaud[1,3] xavier.guillaud@centralelille.fr

Bénédicte Silvestre[5]
benedicte.silvestre.jv@valeo.com

[1]Univ. Lille, ULR 2697 - L2EP, F-59000 Lille, France
[2]Arts et Metiers Institute of Technology, F-59000 Lille, France
[3]Centrale Lille, F-59000 Lille, France
[4]Junia, F-59000 Lille, France
[5]Valeo Siemens e-Automotive, 14 Avenue des Béguines, 95800, Cergy, France

***Abstract*—Nowadays, the production of electric energy is evolving towards decentralized systems by an increasingly advanced integration of new active loads such as electric vehicles and renewable energy sources. This energy transition involves the use of power electronics converters to regulate energy exchanges. In this context, this paper brings the L2EP knowledge on grid-forming control developed in a high-voltage context to the ValeoSiemens reversible charger. This comprises two significant differences in the sizing of the system: a lower grid connection impedance and a resistive aspect of the distribution network. To overcome these challenges, this paper proposes two techniques: the virtual impedance to compensate the low value of connection impedance and dynamic decoupling of active and reactive power to consider the resistive effect of the distribution network.**

***Index Terms*—Distribution Grid, Grid-Forming, Reversible Battery Charger, Voltage Control.**

I. Introduction

The energy evolution aims to invent an energy system that respects the intended zero-carbon neutrality in 2050, the goal stated by the European Union [1]. As this revolution gathers paces, there is a prerequisite to acclimatize the electrical network to withstand the upward energy request sustainably. One of the main challenges of such transition is compensating for Renewable Energy Sources' (RES) intermittent and uncontrollable nature. Due to the climate chain's contributions to mobility, the automotive sector must also evolve towards zero-carbon neutrality. Thus, thermal vehicles are increasingly being replaced with Electric Vehicles (EVs). The connection of an EV to the grid was viewed as a significant opportunity to address the two issues of intermittency and controllability. On this basis, the Power Electronic (PE) converter connected at the grid interface plays a fundamental role in controlling the energy transfer [2]. Indeed, the EV's battery charger linked to the PE converter must be made reversible to allow a part of the energy stored to be returned to the grid. For this aim, this paper covers several operation modes, which can be divided into two major categories (See Fig. 1.):

- Vehicle-to-Grid (V2G): the EV is connected to the grid and allows it to be reinforced by a set of system services.
- Vehicle-to-Load (V2L), Vehicle-to-Home (V2H), Vehicle-to-Building (V2B): the charger or a set of several chargers recreates a micro-grid (islanded situations). Such applications are called self-consumption.

These approaches can be combined and referred to as Vehicle-to-Everything (V2X) to respond vigorously to the system state. This article constitutes a preparatory work for such controls of the reversible chargers.

The charger studied is designed by ValeoSiemens e-Automotive (VSeA). It is the new generation of high power embedded chargers with reversible functionalities. Its entire structure is presented in Fig. 1. This charger is compatible with both single-phase and three-phase power grids. In this paper, only the three-phase case will be studied. For the sake of simplicity, the capacitor, the DC/DC converter, and the battery will be replaced by a constant voltage source $V_{DC} = 800$ V, (supposedly maintained constant by the DC/DC converter). Furthermore, the Electromagnetic Compatibility (EMC) filter will be disregarded.

A PE converter can control either the current acting as a current source or the voltage acting as a voltage source. Traditionally, the network imposes the voltage and the frequency from the power plants. Thus, any active load reported to the network; specifically a PE converter, operates in "grid-following", i.e., controlling a current in phase with the voltage already monitored by the network [3]. In the literature, this type of control is also known as Power Factor Control (PFC). This PFC remains valid and widely used in the EVs world. However, in some other operating modes, the network situation is too weak. Indeed, the distribution station may be located far from the consumption station. Furthermore, in some cases, it can be absent, i.e., in island modes. Consequently, the grid-following control can present instability issues. In this context, it is deemed necessary to switch into a control mode that

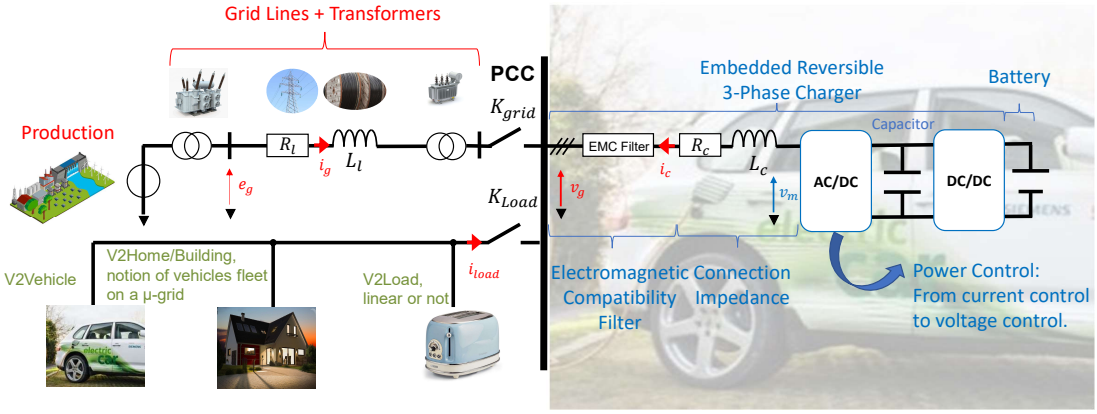

Fig. 1. Functional specifications of the automotive reversible charger.

allows the converter to generate and control the sinusoidal voltage wave. Hence, it is called "grid-forming" control. An example of grid-forming operation on the V2G charger can be found in [4], by switching from current control to voltage control based on the system state. Another voltage control was implemented in an EV charger by using the reactive power compensation [5]. Besides, [6] presents an EV with a bi-directional charger and PFC features.

In the literature, the grid-forming control exists particularly on the micro-grid management [7]. More recently, they have been taken up in a mode of high-voltage transmission networks, where RES become the majority against the conventional means of energy production. The "Power System Team" at the L2EP has mastered the knowledge of grid-forming at the transmission networks ([8], [9], [10]). Compared to the literature available on grid-forming, this paper focuses on the specific case of the automotive charger. More precisely, by comparaison with previous works observed in litterature about grid-forming, two issues are discussed in this paper:

- The scaling constraint of the embedded charger induces a low value of connection impedance $Z_c = R_c + jX_c$ between the charger and the grid.
- The constraint imposed by the distribution network, whose comparatively resistive aspect necessitates the employment of a more complex model than the one commonly used until now in L2EP works in high voltage transmission grids context.

The rest of the paper is organized as follows: Section II clarifies the model representation and reminds the notion of grid-forming control. In Section III, the concept of adding a Virtual Inductance (VI) at the converter level is revealed. Afterwards, a Dynamic Decoupling (DD) method is evaluated in section IV. These models are developed and tested in the MATLAB-SIMULINK simulation environment.

II. Grid-Forming Control

A. Model Representation

To simplify the study, the system of Fig. 1 is reduced to the elementary case of Fig. 2 where the network is reduced to an

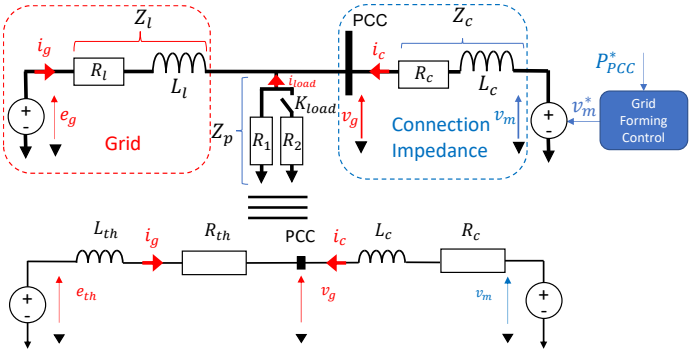

Fig. 2. Equivalent model of the studied system (grid + reversible charger).

equivalent Thévenin model with loads connected in parallel. The charger is represented by a source of modulating voltage v_m and a connection impedance $\underline{Z_c}$. For further simplification, an equivalent system is considered by reducing the load impedance and the grid parameters to the $\underline{Z_{th}}$ impedance and $\underline{E_{th}}$ voltage, according to the expressions illustrated in (1), (2), (3), and (4).

$$\underline{E_{th}} = \frac{\underline{E_g Z_p}}{\underline{Z_l} + \underline{Z_p}} \tag{1}$$

$$\underline{Z_{th}} = \frac{\underline{Z_p Z_l}}{\underline{Z_p} + \underline{Z_l}} \tag{2}$$

$$R_{th} = \frac{R_p\left(R_l^2 + X_l^2\right) + R_l(R_p^2 + X_p^2)}{\left(R_p + R_l\right)^2 + \left(X_p + X_l\right)^2} \tag{3}$$

$$X_{th} = \frac{X_p\left(R_l^2 + X_l^2\right) + X_l(R_p^2 + X_p^2)}{\left(R_p + R_l\right)^2 + \left(X_p + X_l\right)^2} \tag{4}$$

A three-phase converter has been used. Each lowercase notation refers to a set of three-phase references. For example, v_m denotes v_{m_a}, v_{m_b}, and v_{m_c}. Regarding the uppercase symbolization, V_m stands for the RMS values.

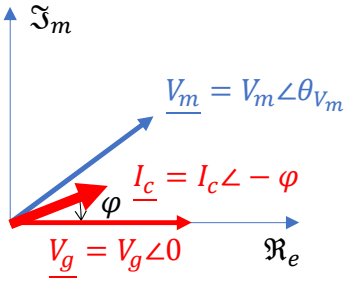

Fig. 3. Vector diagram.

B. Grid-Forming Principle

Within the standard case of an automotive charger, the exchange of active and reactive power with the network is formulated with the expressions of (5) and (6), where $\cos\varphi$ is the power factor. For the rest of the article, it should be noted that the blue color designates the controlled values, and the red color is dedicated to the imposed values.

$$P_{PCC} = V_g I_c \cos\varphi \tag{5}$$

$$Q_{PCC} = V_g I_c \sin\varphi \tag{6}$$

This is the first formulation of P_{PCC} and Q_{PCC} where the charger behaves as a current source by controlling $I_c \cos\varphi$ and $I_c \sin\varphi$. In the case of a weak or absent network, controlling the current on the network may be difficult and causes instability issues. It is therefore necessary to evaluate a new formulation by considering that the charger is no more a controllable source of current, but a source of modulable voltage. Consequently, in the new formulation, the model of $\underline{I_c}$ is considered to incorporate the modulated voltage $\underline{V_m}$ into the expression of active and reactive power. $\underline{I_c}$ is replaced by the expression illustrated in (7) (See Fig. 3):

$$\underline{I_c} = I_c e^{-j\varphi} = \frac{\underline{V_m} - \underline{V_g}}{\underline{Z_c}} \tag{7}$$

Afterward, the expressions of P_{PCC} and Q_{PCC} become the ones expressed in (8) and (9):

$$P_{PCC} = \frac{V_g}{R_c^2 + X_c^2}\left(R_c\left(V_m - V_g\right) + X_c V_m \psi\right) \tag{8}$$

$$Q_{PCC} = \frac{V_g}{R_c^2 + X_c^2}\left(-R_c V_m \psi + X_c\left(V_m - V_g\right)\right) \tag{9}$$

It is noteworthy that the paper's purpose is to transfer the grid-forming "L2EP" knowledge from the transmission system toward the application of the automotive battery charger on the distribution networks. Therefore, the reference case is the typical one observed on a transmission system. In this context, Table I denotes a high connection inductance related to the transformer that connects the PE converter to the PCC. This inductance dominates $\underline{Z_c}$. Consequently, R_c can be neglected in (8) and (9). The expression of P_{PCC} and Q_{PCC} becomes the ones of (10) and (11):

$$P_{PCC} = \frac{V_m V_g}{X_c}\psi \tag{10}$$

TABLE I
REFERENCE SYSTEM PARAMETERS

Symbol	Quantity	Symbol	Quantity
$P_n = S_{n3\varphi}$	22 KW	$X_{c_{ref}} = 10R_c$	0.15 p.u.
V_{bat}	800 V	f_n	50 Hz
w_b	$2\pi * f_n$	$t_{r_{95}}$	0.1 s
Z_l	0.1 p.u.	P_{R_1}	0.5 p.u.
X_l	10R$_l$	P_{R_2}	0.25 p.u.

TABLE II
GRID EVENTS

t (s)	P^* (p.u.)	K_{Load} (logic state)
0	0.2	0
0.5	0.4	0
1.5	-0.1	0
2.5	0.6	0
3.5	0.6	1

$$Q_{PCC} = \frac{V_g}{X_c}\left(V_m - V_g\right) \tag{11}$$

Besides, the transmission case represents a low ratio $\frac{R_l}{X_l}$ that is distinguishable on the transmission lines (aerial lines) for efficiency purposes. These inductive lines make the RMS value V_g less affected by network parameters. However, some alterations will take place in sections III and IV by assuming the case of low voltage automotive charger, for which the model cannot be simplified from equations (8)-(9) to equations (10)-(11). Any modification to the values will be clarified in the corresponding section.

The system is tested on the basis of events in order to validate the defined case study. The PCC now has two resistive loads. Different types of events were addressed in order to test the model's behavior in various conditions. To control a bidirectional energy flow, both positive and negative active power references were handled. It relates to the charging and discharging process in the case of the charger. A load disconnect is also included to allow the response behavior to be consulted with such conduct. Those specifications are fulfilled in Table II (See Fig. 2).

III. Virtual Inductance

According to (8) and (9), a large value of X_c makes the control more resilient against the perturbation on $\underline{V_g}$. $\underline{Z_c}$ corresponds to the transformer leakage inductance. It is designed at a relatively high value for protection purposes: typically 0.15 p.u. with $X_c > 10R_c$ for high voltage transmission lines. In this situation, the control system is thought to be more robust and less susceptible to disruptions. It leads to the definition of the "reference case". The high value of the inductance plays a significant role that allows to assume $V_g = 1$ p.u. in control parameters computations. It makes the control system less sensitive to the unknown change in grid parameters.

The active power control adopted is the conventional droop-based grid-forming control (without PLL) ([10], [12]). The control system is structured in Fig. 4. By considering $V_g = 1$, and $V_m = 1$, the gain m_p is calculated as illustrated in (12),

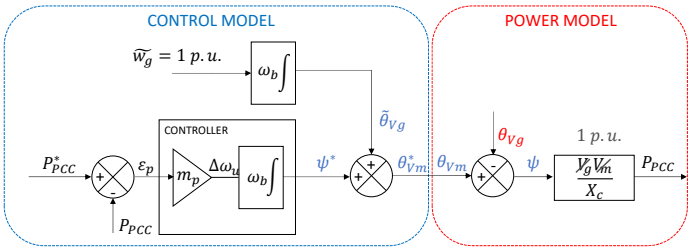

Fig. 4. Partial model of a converter with a grid-forming active power control.

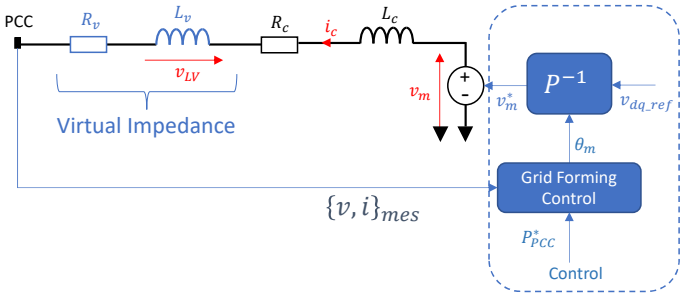

Fig. 5. Add a Virtual Inductance at the converter level.

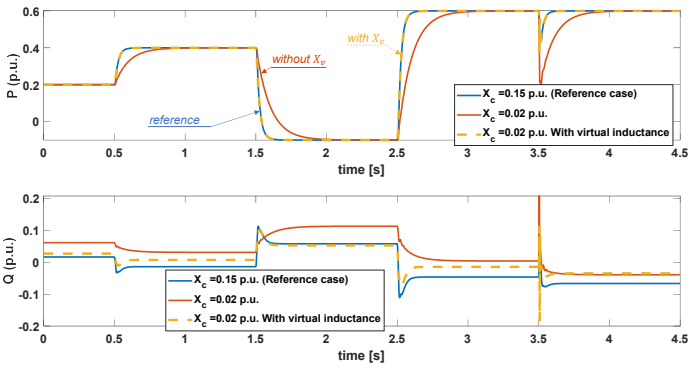

Fig. 6. Effect of the Virtual Inductance on the response of the system.

where $t_{r_{95}}$ is the time response requested. As far as reactive power control is concerned, it is chosen to keep $V_m = 1$ p.u.. For the tests showed in this papers, it permits the converter to furnish the reactive power requested without restrictions.

$$m_p = \frac{3X_c}{t_{r_{95}}\omega_b} \tag{12}$$

However, by connecting a bi-directional battery charger at the distribution level, no transformer is instigated to connect the charger to the PCC. For example, ValeoSiemens uses SiC chips which aim to reduce the size of the passive elements, especially the inductor coils. Thus, the connection reactance is designed for PFC purpose, at a low value, typically below 0.02 p.u., very far from the reference case ($X_c = 0.15$ p.u.). In this case, if the same type of control in Section II is applied, the result moves away from the reference case, as it is showcased in red in Fig. 6. Indeed, as proved in (8) and (9), if X_c is too small, then the control of P_{PCC} is performed with a very small phase shift between $\underline{V_m}$ and $\underline{V_g}$. This makes the control system too sensitive to any disturbance imposed on $\underline{V_g}$, which, in turn, is likely to be more disturbed in a weak situations. Thus, V_g can not be considered equal to 1 p.u.. In a nutshell, the smaller X_c is, the more sensitive the control will be to the defect on $\underline{V_g}$. Hence, this reduction in the connection inductance directly impacts the control system and raises the sensibility to the grid parameters. Thus, to reach the required time response, the value of $\underline{Z_c}$ must dominate the one of the grid. This section aims to restore the value of the lost inductance.

The first solution that can be anticipated is adding a genuine inductance with a very high value. Nevertheless, this implies a bulk and an on-board mass, which is refused to do, especially for an embedded reversible charger application. Accordingly, this section illustrates the method of adding a new one virtually at the converter level. The usage of VI is already a topic that has been discussed in the literature in other circumstances. For example, it is used transiently to protect against over-currents [13]. In this case, the use is permanent in order to address the issue of X_c's low value. As dedicated in Fig. 5, the addition of the VI X_v entails manipulating the voltage reference in order to add the associated terms that are equivalent to the voltage at the terminal of a real inductance. In order to implement the required voltage value, here is a quick reminder of voltage equations in the Park frame:

$$v_{m_d} = v_{g_d} + R_c i_{c_d} + \frac{L_c}{w_b}\frac{di_{c_d}}{dt} - L_c w_g i_{c_q} \tag{13}$$

$$v_{m_q} = v_{g_q} + R_c i_{c_q} + \frac{L_c}{w_b}\frac{di_{cq}}{dt} + L_c w_g i_{c_d} \tag{14}$$

Where w_g is the grid frequency. In this paper, the ideal value is considered ($w_g = 1$ p.u.).

For the sake of the analysis simplicity, the transient part of i_d and i_q is neglected. Thus, $-L_c w_g i_{c_q}$ and $L_c w_g i_{g_d}$ are the parts of the voltage associated with the connection inductance. Subsequently, in order to take into account the supplementary inductance, the terms $-L_v w_g i_d$ and $L_v w_g i_q$ must be added to v_{m_d} and v_{m_q}, respectively, where L_v is the VI. The VI is chosen as the difference between the inductance ($X_{c_{ref}} = 0.15$ p.u) presented in Table I and the actual inductance at the distribution level ($X_c = 0.02$ p.u.).

Alongside the operation of VI, a virtual resistance R_v is transiently added to damp the oscillations that may appear in the transient state. This resistance does not impact the steady-state of the system. More detailed information about this phenomenon can be found in [12] and [14].

As illustrated in Fig. 6, the process of VI and virtual transient resistance allows the system to follow up the reference case of the transmission network. It restores the robustness of the control system against the grid parameters.

IV. Dynamic Decoupling

A. Dynamic Decoupling

By comparison with the reference transmission case, the cables used at the distribution level have different behavior than the ones used in transmission applications. The ratio $\frac{X_l}{R_l}$

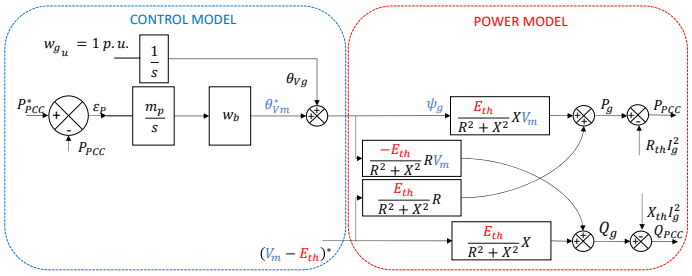

Fig. 7. System model showing the coupling effect between the P_g and Q_g.

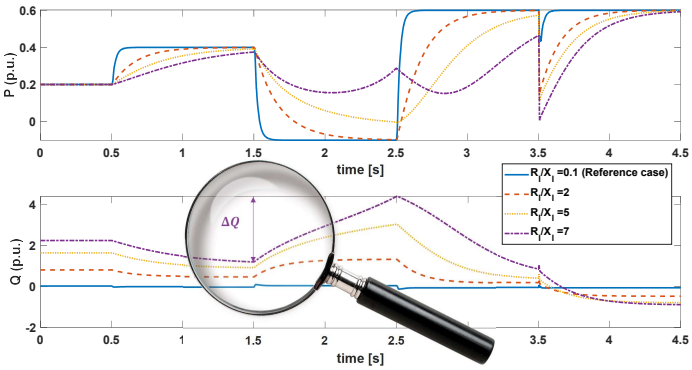

Fig. 8. $\frac{R_l}{X_l}$ parmetrical study with Z_l = 0.1 p.u.

is lower than one. According to the data provided in [15], the system developed in this section (except for the parametrical study) is simulated under a ratio $\frac{R_l}{X_l} = 4.45$. Consequently, the premise that the line resistance R_l should be abandoned is no longer true. This resistance leads to a lack of accuracy in the model proposed in (10) and (11). Because of the intricacy and non-linearity of V_g, a novel representation of the power model is considered. It counts on modeling the entire system by controlling the exchanged power between v_m and e_{th}. The expression of P_g and Q_g are as follows:

$$P_g = \frac{E_{th}}{R^2+X^2}\left(R\left(V_m - E_{th}\right) + XV_m\psi_g\right) \tag{15}$$

$$Q_g = \frac{E_{th}}{R^2+X^2}\left(-RV_m\psi_g + X\left(V_m - E_{th}\right)\right) \tag{16}$$

$$P_{PCC} = P_g - R_{th}I_g^2 \tag{17}$$

$$Q_{PCC} = Q_g - X_{th}I_g^2 \tag{18}$$

$$R = R_{th} + R_c \tag{19}$$

$$X = X_{th} + X_c + X_v \tag{20}$$

$R_{th}I_g^2$ and $X_{th}I_g^2$ are considered constant in steady-state.

No simplifications can be performed on the equations showcased in (15) and (16). Consequently, the control model used in Fig. 7 is not the suitable one for this case. This directs to an increase of the coupling effect between the active and reactive power with the increase of the ratio $\frac{R_l}{X_l}$, as proved in Fig. 8.

To overcome this coupling issue, some decoupling methods have been published in the literature [16], [17]. These methods require the recognition of the ratio $\frac{R}{X}$ and the module

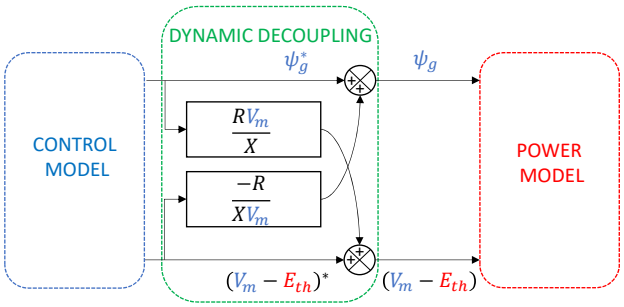

Fig. 9. Dynamic Decoupling implementation.

$Z = \sqrt{R^2+X^2}$. This dependency on Z reduces the system's forcefulness. To the best of the authors' knowledge, no methods have been anticipated without the knowledge of the grid parameters. In this paper, a novel technique of decoupling known as "Dynamic Decoupling" will be described, which requires simply the knowledge of the $\frac{R}{X}$. Moreover, the obtainability of this ratio is not so challenging since it varies slightly from a distribution grid to another.

The DD method consists of adding instantly (See Fig. 9):

- The term $\frac{RV_m}{X}$ to the first new entry of the physical system ψ_g^*.
- The term $\frac{-R}{XV_m}$ to the second new entry of the physical system $(V_m - E_{th})^*$.

After applying the decoupling, the active and reactive power expressions resemble the model simplified under the assumptions of the transmission grid reference case (10)-(11):

$$P_g = \frac{V_m E_{th}}{X}\psi^* \tag{21}$$

$$Q_g = \frac{E_{th}}{X}\left(V_m - E_{th}\right)^* \tag{22}$$

Consequently, this decoupling method allowed the active power to be solely controlled by ψ^*, and the reactive power to be solely controlled by $(V_m - E_{th})^*$. With the implementation of the virtual impedance, this process certified the restoration of the system to its reference modulation, which means a model with no dependency on the resistance value. As proven by the simulation in Fig. 10, the coupling factor falls at t = 0.5 s, t = 1.5 s, and t = 2.5 s. The residual coupling, however, is not a flaw in the suggested method because it is also observed in the reference example. It should be noticed that the large shift in reactive power value at t = 3.5 s has nothing to do with the coupling issue. It is primarily caused by the disconnect of the resistive load. Indeed, according to the Thévenin model represented in (1), (2), (3), (4), and Fig. 2, such disconnection updates the power utilized by the charge.

To prove the forcefulness and the robustness of the proposed methods, the parametrical study shown in Fig. 8 have been re-simulated after implementing the VI and DD. The results are established in Fig. 11. This leads to the same conclusions drawn for Fig. 10. The new architecture proposed proved its effectiveness for a wide range of $\frac{R_l}{X_l}$. Therefore, the decoupling method brings back the reference case studied in section II.

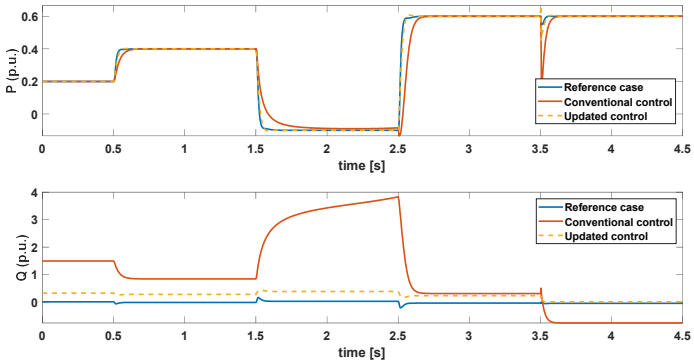

Fig. 10. Dynamic Decoupling effect on active and reactive Power responses.

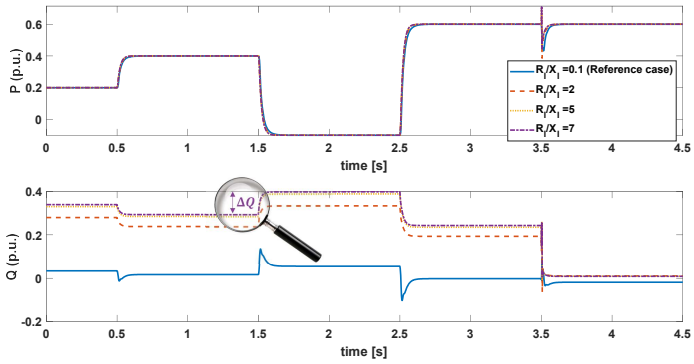

Fig. 11. $\frac{R_l}{X_l}$ parametrical study after decoupling with Z_l = 0.1 p.u.

V. Conclusion

Briefly speaking, the role of transporting electricity to the end customer has evolved with the development of decentralized production of RES. In the context of the citizens' aspiration to energy autonomy, the possibility of integrating storage elements and EVs with reversible battery charger features has increased. At the beginning of this paper, a reminder of the conventional grid-forming architecture on transmission networks took place. To come back to the objective of the article, i.e., to recover an automotive charger control similar to the reference case, two issues were discussed: a small connection impedance X_c and a high $\frac{R_l}{X_l}$ ratio. To overcome the connection impedance issue, the concept of adding a VI was covered to reestablish a conformability between the accurate system time response and the desired one. Besides, the paper interpreted the inherent advantages of a new decoupling method called "Dynamic Decoupling". It certified the restoration of response similar to the one of an inductive line, i.e., a decoupled response of active and reactive power. The experimental verification of the suggested model will shortly be validated on a ValeoSiemens demonstrator, and it will be published in a future publication as part of the planned future projects. Furthermore, as indicated in the introduction, this paper constitutes preliminary work. Further studies will be held on the consolidation of the control architecture by taking all the elements known at the L2EP about grid-forming (quasi-static or dynamic frequency support, current limitation, operation on unbalanced networks, etc.) to allow the charger to work in a variety of industrial circumstances.

Acknowledgment

This work was supported as part of a collaboration between the L2EP laboratory and Valeo Siemens e-Automotive (VSeA), financed by the French investment bank (BPI) through the support plan for the automotive sector: MOBISIC program.

References

[1] European Commission. Directorate-General for Energy, "Energy: roadmap 2050". LU: Publications Office, 2012. [Online]. Available: https://ec.europa.eu [Accessed: April 12, 2021].

[2] J. M. Carrasco et al., "Power-Electronic Systems for the Grid Integration of Renewable Energy Sources: A Survey," in *IEEE Transactions on Industrial Electronics*, vol. 53, no. 4, pp. 1002-1016, June 2006

[3] J. F. Patarroyo-Montenegro, J. D. Vasquez-Plaza, F. Andrade, and L. Fan, "An Optimal Power Control Strategy for Grid-Following Inverters in a Synchronous Frame," *Appl. Sci.*, vol. 10, no. 19, p. 6730, Sep. 2020.

[4] Tan, Kang Miao, Sanjeevikumar Padmanaban, Jia Ying Yong, and Vigna K. Ramachandaramurthy. "A Multi-Control Vehicle-to-Grid Charger with Bi-Directional Active and Reactive Power Capabilities for Power Grid Support." *Energy* 171 (March 2019): 1150–63.

[5] Yong, Jia Ying, Vigna K. Ramachandaramurthy, Kang Miao Tan, and N. Mithulananthan. "Bi-Directional Electric Vehicle Fast Charging Station with Novel Reactive Power Compensation for Voltage Regulation." *International Journal of Electrical Power Energy Systems*, 64 (January 2015): 300–310.

[6] Kim, Seonghye, and Feel-soon Kang. "Multi-Functional On-Board Battery Charger for Plug-in Electric Vehicles." *IEEE Transactions on Industrial Electronics*, 2014, 1–1.

[7] J. Matevosyan et al., "Grid-Forming Inverters: Are They the Key for High Renewable Penetration?," *IEEE Power Energy Mag.*, vol. 17, no. 6, pp. 89–98, Nov. 2019

[8] Taoufik Qoria, Quentin Cossart, Chuanyue Li, Xavier Guillaud, Frederic Colas, François Gruson, Xavier Kestelyn, "WP3 - Control and Operation of a Grid with 100 Converter-Based Devices Deliverable 3.2: Local control and simulation tools for large transmission systems", *H2020 MIGRATE project*, https://www.h2020-migrate.eu/

[9] T. Qoria, E. Rokrok, A. Bruyere, B. Francois, and X. Guillaud, "A PLL-Free Grid-Forming Control With Decoupled Functionalities for High-Power Transmission System Applications," *IEEE Access*, vol. 8, pp. 197363–197378, 2020.

[10] E. Rokrok, T. Qoria, A. Bruyere, B. Francois, and X. Guillaud, "Effect of Using PLL-Based Grid-Forming Control on Active Power Dynamics Under Various SCR," in *IECON 2019 - 45th Annual Conference of the IEEE Industrial Electronics Society*, Lisbon, Portugal, Oct. 2019, pp. 4799–4804.

[11] IEA (2021), Conditions and requirements for the technical feasibility of a power system with a high share of renewables in France towards 2050, IEA, Paris https://www.iea.org/reports/conditions-and-requirements-for-the-technical-feasibility-of-a-power-system-with-a-high-share-of-renewables-in-france-towards-2050.

[12] T. Qoria, "Grid-forming control to achieve a 100 power electronics interfaced power transmission systems," *HESAM University*, 2020.

[13] T. Qoria, F. Gruson, F. Colas, G. Denis, T. Prevost and X. Guillaud, "Critical Clearing Time Determination and Enhancement of Grid-Forming Converters Embedding Virtual Impedance as Current Limitation Algorithm," in *IEEE Journal of Emerging and Selected Topics in Power Electronics*, vol. 8, no. 2, pp. 1050-1061, June 2020.

[14] T. Qoria, C. Li, K. Oue, F. Gruson, F. Colas, and X. Guillaud, "Direct AC voltage control for grid-forming inverters," *J. Power Electron.*, vol. 20, no. 1, pp. 198–211, Jan. 2020.

[15] Nexans Olex New Zealand, "Power Cable Catalogue" 2012 Edition.

[16] K. De Brabandere, B. Bolsens, J. Van den Keybus, A. Woyte, J. Driesen, and R. Belmans, "A Voltage and Frequency Droop Control Method for Parallel Inverters," *IEEE Trans. Power Electron.*, vol. 22, no. 4, pp. 1107–1115, Jul. 2007.

[17] P. Unruh and T. Gühna, "Distributed grid-forming inverters in power grids," p. 8, Nov 2017